Combination of fast-ion diagnostics in velocity-space tomographies

M. Salewski[1], B. Geiger[2], S.K. Nielsen[1], H. Bindslev[3], M. García-Muñoz[2], W.W. Heidbrink[4], S.B. Korsholm[1], F. Leipold[1], J. Madsen[1], F. Meo[1], P.K. Michelsen[1], D. Moseev[2,5], M. Stejner[1], G. Tardini[2], and the ASDEX Upgrade team[2]

[1] Association Euratom - DTU, Technical University of Denmark, Department of Physics, DTU Risø Campus, DK-4000 Roskilde, Denmark

[2] Association Euratom - Max-Planck-Institut für Plasmaphysik, D-85748 Garching, Germany

[3] Aarhus University, Faculty of Science and Technology, DK-8000 Aarhus C, Denmark

[4] University of California, Irvine, Department of Physics and Astronomy, California 92697, USA

[5] Association Euratom - FOM Institute DIFFER, 3430 BE Nieuwegein, The Netherlands

E-mail: `msal@fysik.dtu.dk`

Abstract. Fast-ion D_α (FIDA) and collective Thomson scattering (CTS) diagnostics provide indirect measurements of fast-ion velocity distribution functions in magnetically confined plasmas. Here we present the first prescription for velocity-space tomographic inversion of CTS and FIDA measurements that can use CTS and FIDA measurements together and that takes uncertainties in such measurements into account. Our prescription is general and could be applied to other diagnostics. We demonstrate tomographic reconstructions of an ASDEX Upgrade beam ion velocity distribution function. First, we compute synthetic measurements from two CTS views and two FIDA views using a TRANSP/NUBEAM simulation, and then we compute joint tomographic inversions in velocity-space from these. The overall shape of the 2D velocity distribution function and the location of the maxima at full and half beam injection energy are well reproduced in velocity-space tomographic inversions, if the noise level in the measurements is below 10%. Our results suggest that 2D fast-ion velocity distribution functions can be directly inferred from fast-ion measurements and their uncertainties, even if the measurements are taken with different diagnostic methods.

PACS numbers: 52.25.Os, 52.40.Db, 52.50.Gj, 52.65.Cc, 52.70.Gw, 52.70.Kz

1. Introduction

ASDEX Upgrade is a medium-size tokamak that is equipped with powerful and versatile auxiliary heating systems: A variety of fast-ion populations can be generated by eight neutral beam injection (NBI) sources with a total power of 20 MW and four ion cyclotron resonance heating (ICRH) antennas with a total power of 6 MW [1–3]. ASDEX Upgrade is also equipped with a suite of fast-ion diagnostics: fast-ion loss detectors (FILD) [4–6], fast-ion D_α (FIDA) [7], collective Thomson scattering (CTS) [8–13], neutron spectrometry [14, 15], neutral particle analyzers (NPA) [16, 17], and γ-ray spectrometry [18]. These auxiliary heating systems and fast-ion diagnostics give unique opportunities to study fast ions in tokamak plasmas. Each diagnostic observes fast ions in different, restricted parts of configuration space and velocity space. CTS and FIDA diagnose confined fast ions in small volumes relative to the plasma size. FILDs are sensitive to lost fast ions near the plasma edge that strike the scintilator plates. Passive NPAs, neutron spectrometers, and γ-ray spectrometers detect confined fast ions anywhere along the lines-of-sight.

We focus here on CTS and FIDA measurements that could be made at roughly the same location in configuration space. CTS and FIDA measure spectra of scattered and emitted radiation, respectively, that constitute 1D functions of the fast-ion velocity distribution function. Traditionally, fast-ion CTS or FIDA measurements are often compared with simulated spectra to investigate if the measurements match the expectation or if they are anomalous [9, 19, 20]. Orbit-following codes such as TRANSP/NUBEAM provide the local 2D fast-ion velocity distribution function f, and then synthetic measurements are calculated from f. However, if the real measurements disagree with the synthetic measurements, it is often unclear what caused this discrepancy. Our final goal is to experimentally determine f, and this might help establish where in 2D velocity space the measurements disagree with the simulation. Inference of tomographic inversions in velocity space from CTS or FIDA measurements was recently shown to be an achievable goal [13]. Velocity-space tomographic inversions are the best fit to the CTS and FIDA measurements under a regularization condition. It was also shown that the resemblance of the inversions with the original 2D ion velocity distribution function improves with the number of available views, and this motivates the combination of CTS and FIDA measurements in joint velocity-space tomographic inversions. Here we derive a new prescription for velocity-space tomography that allows such a combination of diagnostics which was not possible with previous methods [13]. Our new prescription is also the first to account for uncertainty in the individual measurements. Lastly, we here present a method to estimate uncertainty levels in the tomographic inversions.

Among the most wide-spread applications of computed tomography in configuration space are medical imaging, e.g. x-ray computed axial tomography (CAT or CT) scanners, positron emission tomography (PET) scanners or magnetic resonance imaging (MRI) scanners [21, 22], and it is also widely used in nuclear fusion research [23–32].

Velocity-space tomography is less developed [13, 33, 34] but could be particularly useful in studies of selective ejection or redistribution in velocity space. Several types of modes affect ions in only part of velocity space, for example sawteeth [35–38], Alfvén eigenmodes [6, 39–43] and neoclassical tearing modes [4, 5]. Turbulent transport of fast ions also depends on the ion energy [44–47]. Additionally, velocity-space tomography could be used to monitor phase-space engineering of fast-ion velocity distribution functions which has enabled control of sawteeth and neoclassical tearing modes [48].

We compute joint tomographic inversions of 2D fast-ion velocity distribution functions from synthetic 1D CTS and FIDA measurements. The use of synthetic diagnostics gives us the advantage that we can compare the underlying, known 2D velocity distribution functions with the inversions. The synthetic measurements were calculated from a TRANSP/NUBEAM simulation for the combined four-view FIDA/CTS system at ASDEX Upgrade. Our joint tomography method could also combine the fast-ion charge exchange spectroscopy (FICXS) (that detects light other than D_α but is otherwise similar to FIDA) and the CTS diagnostics at LHD [49, 50]. Moreover, joint tomographic inversions could be directly relevant to ITER where the proposed FICXS [51] and the CTS system [52–55] could be combined even if there is only one CTS view. Measurements from any other fast-ion diagnostic could be included in our joint tomography prescription, if quantitative weight functions describing the measurements such as those for CTS [34] or FIDA [20, 56] can be formulated. Our joint tomography method would then also be applicable to other tokamaks with many-view FIDA systems and additional fast-ion diagnostics, for example DIII-D [57, 58], NSTX [59] and MAST. Here we make a start by combining CTS and FIDA.

In section 2 we describe the four-view CTS and FIDA system at ASDEX Upgrade, and in section 3 we discuss the combination of CTS and FIDA measurements and their uncertainties in a joint tomography prescription. Joint tomographic inversions of a simulated beam ion distribution function from combined synthetic CTS and FIDA measurements and their uncertainties are presented in section 4, and in section 5 we study the effect of noise. Finally, we discuss the intrinsically complementary nature of CTS and FIDA measurements in section 6, and we draw conclusions in section 7.

2. CTS and FIDA measurements at ASDEX Upgrade

The CTS system at ASDEX Upgrade has two receivers after installations in 2012, and likewise the FIDA system has two optical heads. CTS and FIDA measurements are sensitive to the velocity-space distribution in small measurement volumes. Except for different shapes and sizes of the measurement volumes, which we ignore here assuming measurements in spatial points, the CTS and FIDA measurements could be made at the same position assuming toroidal symmetry. Hence, four simultaneous views of the 2D fast-ion distribution function are now available if the CTS views and the FIDA views are used together. The spatial resolution of the CTS diagnostic at ASDEX Upgrade is about 10 cm which is given by the size of the intersection pattern of the probe beam from a

gyrotron and the receiver field of view. The measurement positions can be moved freely in the plasma core by means of steerable antennas. The measurement locations of the two CTS views can be similar in the poloidal (R,Z) plane if two probe beams are used. The time resolution is often set to 4 ms given by the gyrotron modulation frequency. The position of a FIDA measurement is determined by the intersection of the NBI S3 beam path and the line-of-sight (LOS) of the optical head. The spatial resolution of the FIDA diagnostic at ASDEX Upgrade is about 7 cm, and the time resolution is 2 ms.

CTS and FIDA measure 1D functions g which depend on the respective projection angles ϕ_{CTS} and ϕ_{FIDA} and the fast-ion 2D velocity-space distribution function f that we assume to be rotationally symmetric about the magnetic field direction. CTS and FIDA weight functions relate the 2D fast-ion velocity distribution function f to the 1D measurements g [34, 56]. CTS and FIDA weight functions w are defined by

$$g_{CTS}(u, \phi_{CTS}) = \int_{-\infty}^{\infty}\int_{0}^{\infty} w_{CTS}(u, \phi_{CTS}, v_\parallel, v_\perp) f(v_\parallel, v_\perp) dv_\perp dv_\parallel, \quad (1)$$

$$g_{FIDA}(\lambda, \phi_{FIDA}) = \int_{-\infty}^{\infty}\int_{0}^{\infty} w_{FIDA}(\lambda, \phi_{FIDA}, v_\parallel, v_\perp) f(v_\parallel, v_\perp) dv_\perp dv_\parallel \quad (2)$$

where u is the projected velocity and λ is the wavelength of detected FIDA light. Examples of weight functions for CTS and FIDA for $\phi_{CTS} = \phi_{FIDA} = 64°$ are shown in figure 1.

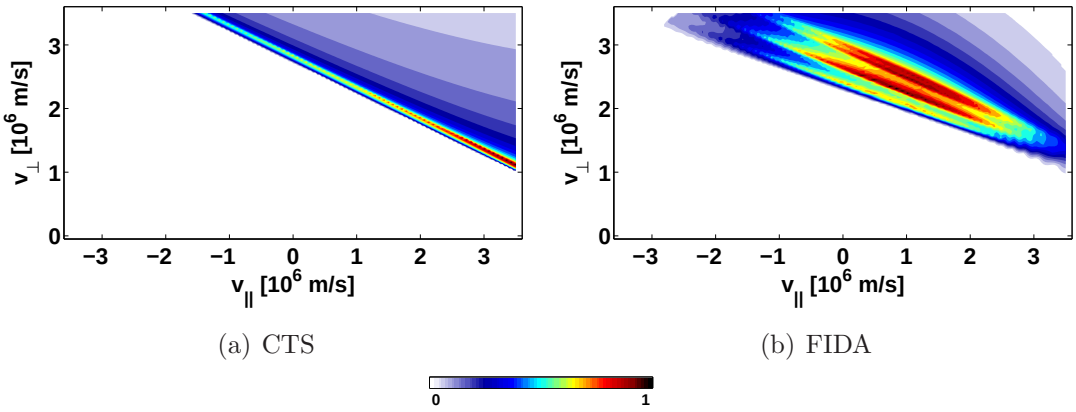

(a) CTS (b) FIDA

Figure 1. Weight functions [a.u.] at a projection angle of $\phi_{CTS} = \phi_{FIDA} = 64°$ for (a) CTS and (b) FIDA and a particular velocity or wavelength interval.

CTS diagnostics are sensitive to 1D projections of f onto the wave vector $\mathbf{k}^\delta = \mathbf{k}^s - \mathbf{k}^i$ which is the difference between the wave vectors of scattered radiation $\mathbf{k}^s$ and incident radiation $\mathbf{k}^i$. The most important angle to describe the pre-selected projection direction given by $\mathbf{k}^\delta$ is the projection angle $\phi_{CTS} = \angle(\mathbf{k}^\delta, \mathbf{B})$ where $\mathbf{B}$ is the magnetic field. A frequency shift ν^δ of scattered radiation can be related to the ion velocity $\mathbf{v}$ projected onto $\mathbf{k}^\delta$:

$$\nu^\delta = \nu^s - \nu^i \approx \mathbf{v} \cdot \mathbf{k}^\delta / 2\pi = u k^\delta / 2\pi \quad (3)$$

where $k^\delta = |\mathbf{k}^\delta|$. We define here a CTS *measurement* as detection of the fast ion phase-space density in a particular interval in u that is related to an interval in ν^δ

via equation 3. The projection angles ϕ_{CTS} of the two CTS views can be varied independently if two probe beams are used.

For FIDA, the fast ions likewise leave a spectral signature in the detected light by Doppler shift and Stark splitting. FIDA weight functions are directly parametrized by the wavelength of detected radiation λ instead of u [20, 56]. Hence we define here as FIDA *measurement* the detection of Doppler- and Stark-shifted light in a particular wavelength interval. The FIDA optical head observes NBI source S3 in the plasma core at two different fixed angles $\phi_{FIDA} = \angle(\mathbf{k}^{LOS}, \mathbf{B})$ where $\mathbf{k}^{LOS}$ is the wave vector along the line-of-sight (LOS) of the optical heads. The toroidal LOS has an angle of $\phi_{FIDA} = 11°$, and the poloidal LOS, that was installed in 2012, has $\phi_{FIDA} = 64°$. The angles ϕ_{CTS} and ϕ_{FIDA} describing the *view*, the measurements g_{CTS} and g_{FIDA}, and the weight functions w_{CTS} and w_{FIDA} are analogous and will hereafter simply be called ϕ, g, and w, respectively. The analogy between CTS and FIDA measurements is reflected in the form of the weight functions that can be chosen to be quite similar as we show in figure 1. We will discuss the differences between the CTS and FIDA weight functions with identical projection angle ϕ in section 6.

3. Prescription for joint tomographic reconstruction from measurements and their uncertainties

We discretize f and the measurements g from CTS and FIDA into f_{kl} and g_{ij} and the coordinates $(u, \phi, v_\parallel, v_\perp)$ into $(u_i, \phi_j, v_{\parallel k}, v_{\perp l})$. The discrete functions f_{kl} and g_{ij} are written into the column matrices F and G, respectively, similarly to the procedure in reference [13]. F is a column matrix of size $N \times 1$ obtained from the discrete 2D fast-ion velocity distribution function described by $N = K \times L$ grid points (K grid points in $v_\perp$ and L in $v_\parallel$). G is a column matrix of size $M \times 1$ consisting of the discrete 1D functions measured with CTS or FIDA. M is the total number of measurements in u_i (CTS) and λ_i (FIDA) made in the J views with projection angles ϕ_j. The subscripts i, j, k, l, m, n run from 1 to the corresponding upper case letter I, J, K, L, M, N. The discretized form of equations 1 and 2 is

$$g_{ij} = \sum_{k=1}^{K} \sum_{l=1}^{L} w_{ijkl} f_{kl} \Delta v_\perp \Delta v_\parallel \tag{4}$$

where $\Delta v_\perp$ and $\Delta v_\parallel$ are the cell sizes in $v_\perp$and $v_\parallel$, respectively. Using these discrete weight functions, we can immediately write down an $M \times N$ transfer matrix W taking F into G [13], and we obtain the linear system of equations

$$WF = G. \tag{5}$$

In real experiments the transfer matrix W and the measurements G are known, and tomographies can be found by solving the inverse problem in equation 5. If the measurements G contain noise, there is no exact solution irrespective of whether the system of equations is underdetermined or overdetermined, but we can find a best fit F^+ by minimizing a figure of merit χ^2. Whereas in reference [13] we assumed identical

uncertainties in all measurements, we here allow for individual uncertainties $\sigma_{G,m}$ in each measurement. For correlated uncertainties in the measurements, the χ^2 figure of merit is determined by the covariance matrix of the measurements C_G and the misfit of the measurements [60]:

$$\chi^2 = \sum_{m,m'} \left(G_m - \sum_n W_{mn} F_n \right) C^{-1}_{G,mm'} \left(G_{m'} - \sum_{n'} W_{m'n'} F_{n'} \right) \tag{6}$$

where the subscribts denote the matrix elements. We here assume the uncertainties to be uncorrelated and get the usual least-square figure of merit in which the misfit of each measurement is divided by its uncertainty:

$$\chi^2 = \sum_m \left(\frac{G_m - \sum_n W_{mn} F_n}{\sigma_{G,m}} \right)^2 = \sum_m \left(\frac{G_m}{\sigma_{G,m}} - \sum_n \frac{W_{mn}}{\sigma_{G,m}} F_n \right)^2 . \tag{7}$$

In matrix form this becomes

$$\chi^2 = \mid \hat{G} - \hat{W} F \mid^2 . \tag{8}$$

The matrix elements of $\hat{G}$ and $\hat{W}$ are given by

$$\hat{G}_m = G_m / \sigma_{G,m} \tag{9}$$

$$\hat{W}_{mn} = W_{mn} / \sigma_{G,m} \tag{10}$$

where repeated indices do *not* imply summation. We find a minimum χ^2 figure of merit under minimum 2-norm regularization and positivity constraint using the Moore-Penrose pseudoinverse $\hat{W}^+$ [61, 62] computed from the singular value decomposition of $\hat{W}$ [63]. Therefore, the tomographic inversion F^+ is determined from the measurements and their uncertainties by

$$F^+ = \hat{W}^+ \hat{G}. \tag{11}$$

F^+ is the least-square-fit to the normalized set of equations

$$\hat{W} F = \hat{G}. \tag{12}$$

In reference [13] the figure of merit was simply

$$\chi^2 = \mid G - W F \mid^2 \tag{13}$$

which is minimized by

$$F^+ = W^+ G \tag{14}$$

as the best-fit solution to equation 5. Equations 5 and 12 are equivalent, but here the figure of merit χ^2 (equation 8) is different than in reference [13] (equation 13). By this normalization of W and G with σ_G we here take the uncertainties of the individual measurements into account. If all uncertainties are equal, the reconstruction prescription in reference [13] is recovered.

The normalization of the measurements and the weight functions by their respective uncertainties is also essential to improve the conditioning of the transfer matrix. Without this normalization the conditioning of W would usually be poor for combined

CTS and FIDA measurements because CTS and FIDA measure different physical quantities, and their weight functions are usually given in different units and have amplitudes that differ by orders of magnitude. The conditioning of $\hat{W}$, on the contrary, should usually be good, and this well-conditioned transfer matrix allows the combination of CTS and FIDA measurements. The singular values before and after the normalization by the uncertainties are shown in figure 2. Here we assume the uncertainty in each view to be 10% of the maximum value of the respective view.

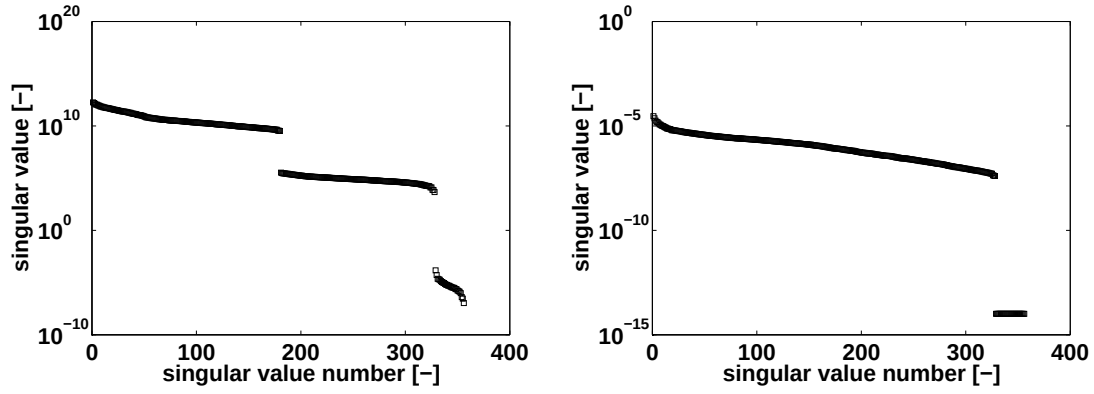

(a) (b)

Figure 2. a) Singular values of the transfer matrix W for combined CTS and FIDA measurements (before normalization with the uncertainties). b) Singular values of the transfer matrix $\hat{W}$ for combined CTS and FIDA measurements (after normalization with the uncertainties).

4. Joint tomographic inversion from combined CTS and FIDA measurements

First we illustrate the data we use for the inference of F^+. Figure 3a shows a beam ion velocity distribution function for NBI source S3 (60 keV, 2.5 MW) at ASDEX Upgrade computed with TRANSP/NUBEAM, and figure 3b shows a set of normalized, synthetic CTS and FIDA measurements of that function. The resolution of the original function, from which we take the synthetic measurements, is 300×601 grid points. The two bumps to the left in figure 3b represent CTS measurements taken in two views at $\phi = (33°, 85°)$, and the two bumps to the right represent FIDA measurements at $\phi = (11°, 64°)$ for the two FIDA views. The CTS measurements are distributed in the u-intervals $-5 \times 10^6 < u < -0.7 \times 10^6$ m/s and $0.7 \times 10^6 < u < 5 \times 10^6$ m/s with a resolution of $\Delta u = 0.1 \times 10^6$ m/s that is roughly achievable with the filterbank receivers at ASDEX Upgrade. We do not use CTS measurements in the interval $-0.7 \times 10^6 < u < 0.7 \times 10^6$ m/s because bulk ions make unambiguous detection of fast ions very difficult if not impossible in this interval. The FIDA measurements are evenly distributed in the wavelength intervals 649 nm $< \lambda <$ 654 nm and 659 nm $< \lambda <$ 663 nm. FIDA light cannot be observed in the wavelength interval 654 nm $< \lambda <$ 659 nm due to

beam emission and halo neutrals [7], and we likewise exclude this wavelength range in the synthetic measurements. Figure 3b contains the synthetic normalized measurements that we use for the inference of the tomographic inversions. The abscissa is the measurement index label m that runs from 1 to M, and the ordinate is the corresponding CTS or FIDA measurement normalized by the uncertainty of the measurement (10% of the maxima of each CTS or FIDA view as explained above).

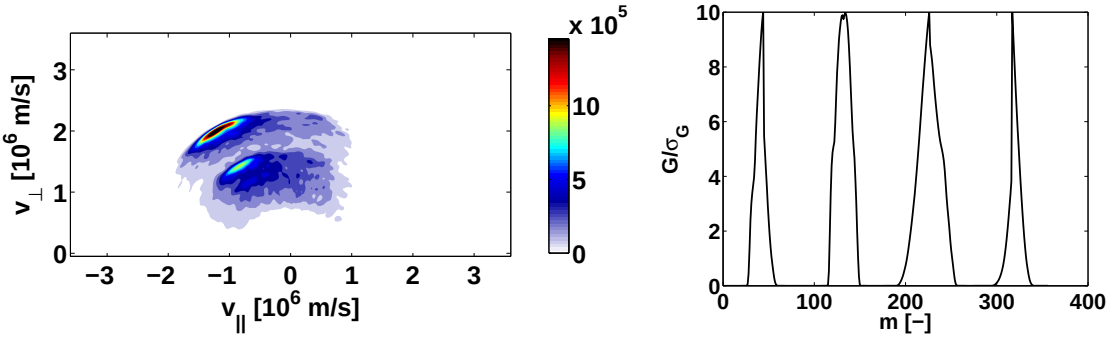

(a) f (b) G

Figure 3. (a) 2D velocity distribution function f on a very fine grid (300×601). (b) Synthetic measurement data in G from two CTS views with $\phi = (33°, 85°)$ (left bumps) and two FIDA views with $\phi = (11°, 64°)$ (right bumps). m is the index of the measurement.

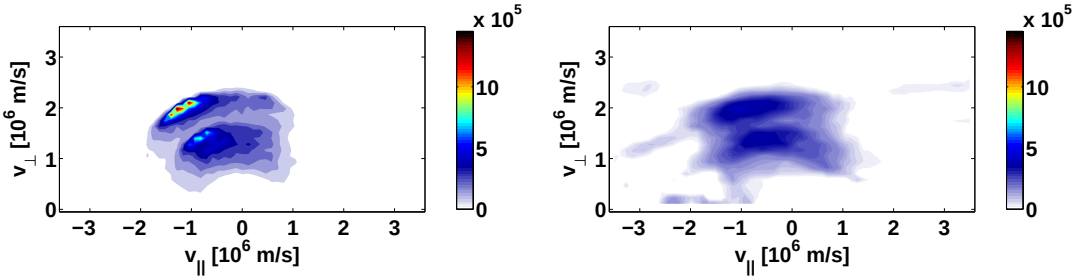

(a) (b) 0%, 200 SV

Figure 4. (a) Interpolation of the original function from figure 3(a) to the 30×61 grid of the tomographic inversion. (b) Inversion using 200 singular values. No additional noise has been added to G. The color scales in (a) and (b) are identical. Figure 5(e) presents the inversion with a different color scale.

The inversions are calculated on a much coarser grid with 30×61 grid points corresponding to velocity-space resolution of typical simulations. The original function has been interpolated to the coarser grid of the inversion in figure 4a to illustrate an upper limit of the achievable resemblance between the inversion and the original function. If the data is noisy, it is necessary to truncate the SVD and use lower rank approximations to the Moore-Penrose pseudoinverse. Explicit noise will be added in section 5 whereas in this section the noise originates from the different discretizations

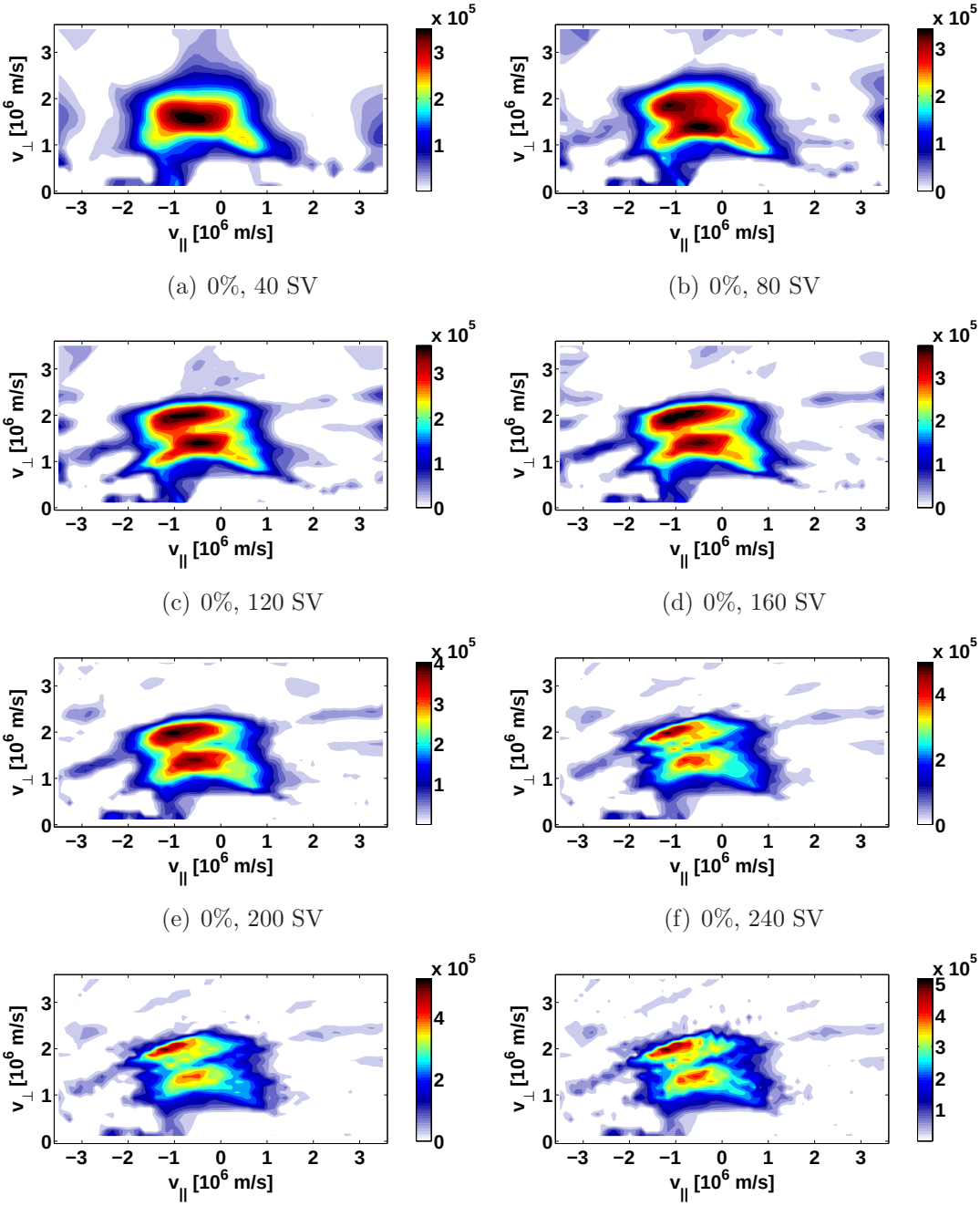

(a) 0%, 40 SV (b) 0%, 80 SV

(c) 0%, 120 SV (d) 0%, 160 SV

(e) 0%, 200 SV (f) 0%, 240 SV

(g) 0%, 280 SV (h) 0%, 320 SV

Figure 5. Tomographic inversions inferred from the synthetic CTS/FIDA four-view data in figure 3(b). 40 - 320 singular values are used in (a) to (h). No additional noise has been added to G. The color scales are different from that of the original in figure 4.

of the original function (300×601) and the inversion (30×61). Here the transfer matrix W has a rank of about 320, corresponding to 320 significant singular values (see figure 2b). In truncated SVD, only the largest singular values are used. Figure 4b shows a inversion using 200 singular values. The joint inversion from a mix of CTS and FIDA measurements reproduces the overall shape of the underlying function including the location of the peaks at full and half beam injection energy. However, these peaks are broader in the inversion than in the original function, and their amplitudes are approximately 3–4 times smaller.

Figure 5 shows inversions computed with various truncation levels from 40 singular values to 320 singular values. From here on we use different color scales in the inversions to emphasize the shape of the inferred inversions more clearly. The two peaks at full and half beam injection energies emerge if about 80 singular values are used. The peak amplitudes become larger if more singular values are used, but they never become quite as large as in the original. Using more singular values, however, also tends to increase the jitter in the inversion.

It should be possible to improve the resemblance of the inversions with the original velocity distribution function by adding more CTS or FIDA views or other fast-ion measurements and by increasing the frequency resolution of the measurements [13]. High frequency resolution CTS measurements on the order of 1 MHz were recently demonstrated which give a few thousand measurements in frequency space per view [64–66].

5. Joint tomographic inversions from noisy measurements

In the following we investigate inversions computed from noisy measurements. Noise makes the smallest singular values useless, and the inversions then have to be inferred using only the largest singular values. The lower the noise level, the more singular values can be used. We add various levels of uncorrelated Gaussian noise to the synthetic measurements and infer inversions at various truncation levels of the SVD.

Figure 6 shows inversions computed for a Gaussian noise level of 2%. The two beam injection peaks again emerge if about 80 singular values are used. About 240 singular values contain useful information at 2% noise. In figure 7 we infer inversions at various noise levels up to 50%. The two peaks at full and half beam injection energy are visible for 100 singular values at noise levels of 4% (figure 7a). At 10% noise (figure 7b), the form of the peaks is distorted by the noise, and for larger noise levels such as 20% they completely disappear (figure 7c) in the jitter. Nevertheless, even at a noise level of 50%, the inversion based on 20 singular values still reveals the coarsest anisotropy features of the original function (figure 7d).

For a matrix equation of the form $F^+ = \hat{W}^+ \hat{G}$, we can investigate the propagation of errors from the normalized measurements $\hat{G}$ to the inversion F^+. The measurements can contain correlated noise that can be summarized in the $m \times m$ covariance matrix $\hat{C}_G$. We then use standard error propagation methods [60] to find the $n \times n$ covariance

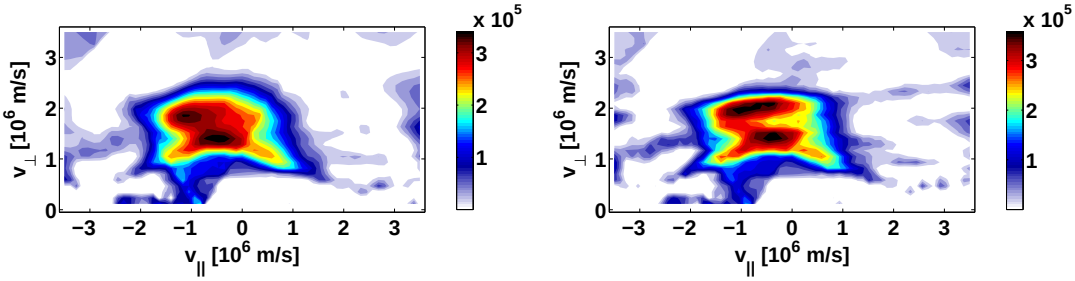

(a) 2%, 80 SV (b) 2%, 140 SV

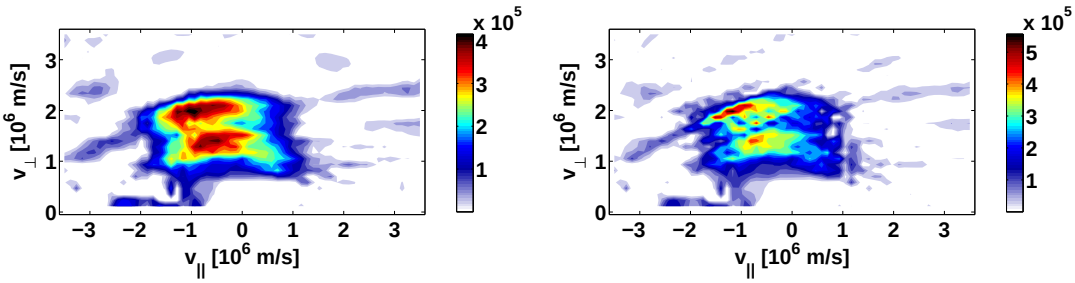

(c) 2%, 200 SV (d) 2%, 240 SV

Figure 6. Tomographic inversions inferred from the synthetic CTS/FIDA four-view data in figure 3(b) with 2% Gaussian noise. 80 - 240 singular values are used. The color scales are different from that of the original in figure 4.

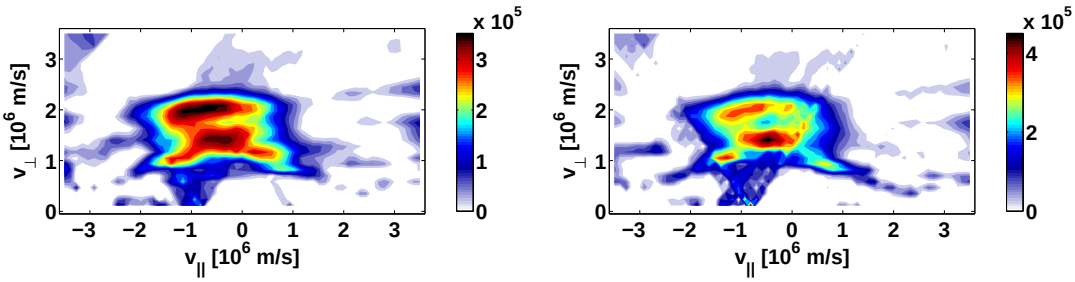

(a) 4%, 100 SV (b) 10%, 100 SV

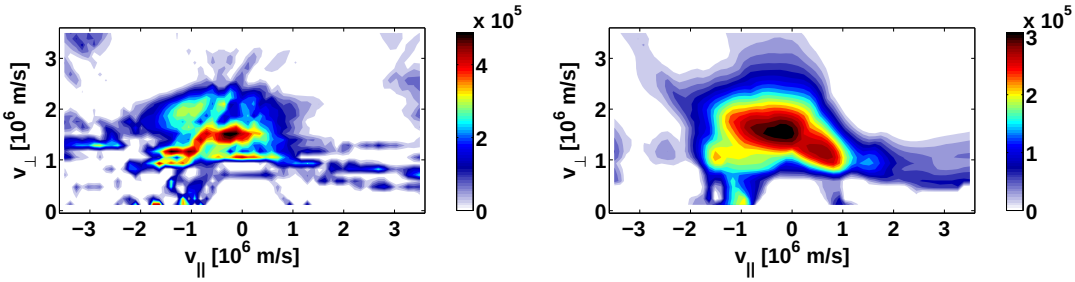

(c) 20%, 100 SV (d) 50%, 20 SV

Figure 7. Tomographic inversions inferred from the synthetic CTS/FIDA four-view data in figure 3(b) with 4% - 50% Gaussian noise. In (a) to (c) we use 100 singular values, in (d) we use 20 singular values. The color scales are different from that of the original in figure 4.

matrix C_F^+ of F^+:

$$C_F^+ = \hat{W}^+ \hat{C}_G (\hat{W}^+)^T. \tag{15}$$

For uncorrelated noise in the measurements, the diagonal elements $(\sigma_{F,n}^+)^2$ of C_F^+ are given by

$$(\sigma_{F,n}^+)^2 = \sum_m (\hat{W}_{nm}^+)^2 \hat{\sigma}_{G,m}^2. \tag{16}$$

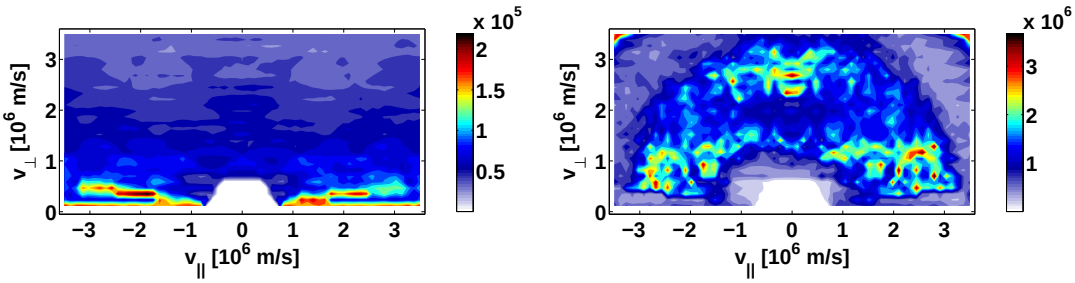

(a) 100 SV (b) 300 SV

Figure 8. Standard deviation σ_f^+ of the inversion obtained from the diagonal elements of the covariance matrix for (a) 100 singular values and (b) 300 singular values.

Figure 8 shows standard deviations σ_f^+, which are immediately given by the vectors σ_F^+, using 100 singular values (a) and 300 singular values (b). Tomographic inferences using only the largest singular values are less sensitive to noise than those using many singular values. For 100 singular values, the values of f are well above the noise level σ_f^+, and hence a tomographic inversion f^+ using 100 singular values is dominated by the measured values g. On the contrary, for 300 singular values, the values of f are below the noise level σ_f^+, and hence this inversion f^+ is strongly influenced by noise.

6. The complementary nature of CTS and FIDA measurements

Lastly, we remark that the velocity-space interrogation regions of CTS and FIDA measurements and the relative weightings within these can in fact never coincide, irrespective of how we choose the scattering geometry. These weightings are described by the weight functions w that relate the 2D velocity-space $(v_\parallel, v_\perp)$ to the 1D CTS or FIDA measurements of a spectrum of radiation. CTS and FIDA measurements g are sensitive to products of their respective weight functions and the ion velocity distribution function f according to equations 1 and 2. The basic shapes of CTS and FIDA velocity-space interrogation regions were illustrated in figure 1. They are given by 1D projections of velocities of gyrating ions determining the frequency shifts of detectable radiation [34]. Despite the identical projection angle in figure 1, the boundaries of the triangular velocity-space interrogation region of FIDA have a smaller slope than those for CTS due to Stark splitting: Stark splitting broadens the FIDA velocity-space interrogation regions compared with those of CTS. The weights are also different due to Stark splitting,

the charge exchange probability, and the probability of a Balmer alpha photon emission. Figure 1 suggests that the observable signals emphasize different velocity-space regions even if the interrogation regions are chosen to be as similar as possible. This makes direct comparisons of CTS and FIDA measurements difficult as these measurements can never be redundant; they are complementary irrespective of the viewing geometry. But the combination of the measurements in joint inversions turns this intrinsically complementary nature of the measurements into an advantage. One may then speculate how to set the projection angles of the available CTS and FIDA views to obtain the best possible inversion and how many views are really required. It is firstly beneficial to increase the number of views and secondly to select very different projection angles in each view as one would intuitively expect. It is, however, outside the scope of the present work to find optimum projection angles or number of views, and we will give comprehensive discussion of these topics elsewhere.

7. Conclusions

We have demonstrated that diagnostic information from CTS and FIDA measurements can be combined in joint velocity-space tomographic inversions that provide the best fit to the measurements under a regularization condition. To enable this combination of diagnostic methods, we have derived a new velocity-space tomography prescription that can use information from any fast-ion diagnostic and that takes uncertainties in the measurements into account. We infer tomographic reconstructions using synthetic measurements with the combined four-view CTS/FIDA system at ASDEX Upgrade. The synthetic measurements are based on a beam ion velocity distribution function simulated with TRANSP/NUBEAM. The overall shape of the distribution function and the location of the maxima at full and half beam injection energy are reproduced well in tomographic inversions, if uncorrelated Gaussian noise in the measurements has a level below 10%. Joint tomography using real fast-ion measurements can combine different diagnostic methods – also other than CTS and FIDA – and can yield an experimentally determined 2D fast-ion velocity distribution function.

Acknowledgements

This work, supported by the European Communities under the contract of Association between Euratom and DTU, was partly carried out within the framework of the European Fusion Development Agreement. The views and opinions expressed herein do not necessarily reflect those of the European Commission.

References

[1] O. Gruber. Overview of ASDEX Upgrade results. *Nuclear Fusion*, 47(10):S622–S634, October 2007.

[2] A. Kallenbach, V. Bobkov, F. Braun, A. Herrmann, H. Hohnle, R.M. McDermott, R. Neu, J. Noterdaeme, T. Putterich, J. Schweinzer, J. Stober, E. Strumberger, W. Suttrop, D. Wagner, and H Zohm. Recent ASDEX Upgrade Results and Future Extension Plans. *IEEE Transactions on Plasma Science*, 40(3):605 – 613, 2012.

[3] U. Stroth et al. Overview of ASDEX Upgrade Results. *Nuclear Fusion*, (Special issue: FEC2012 Overview), in press.

[4] M García-Muñoz, P Martin, H.-U Fahrbach, M Gobbin, S Günter, M Maraschek, L Marrelli, H Zohm, and the ASDEX Upgrade Team. NTM induced fast ion losses in ASDEX Upgrade. *Nuclear Fusion*, 47(7):L10–L15, July 2007.

[5] M. García-Muñoz, H.-U. Fahrbach, S.D. Pinches, V. Bobkov, M. Brüdgam, M. Gobbin, S. Günter, V. Igochine, Ph. Lauber, M.J. Mantsinen, M. Maraschek, L. Marrelli, P. Martin, P. Piovesan, E. Poli, K. Sassenberg, G. Tardini, and H. Zohm. MHD induced fast-ion losses on ASDEX Upgrade. *Nuclear Fusion*, 49(8):085014, August 2009.

[6] M. Garcia-Munoz, I.G.J. Classen, B. Geiger, W.W. Heidbrink, M.A. Van Zeeland, S. Äkäslompolo, R. Bilato, V. Bobkov, M. Brambilla, G.D. Conway, S. da Graça, V. Igochine, Ph. Lauber, N. Luhmann, M. Maraschek, F. Meo, H. Park, M. Schneller, and G. Tardini. Fast-ion transport induced by Alfvén eigenmodes in the ASDEX Upgrade tokamak. *Nuclear Fusion*, 51(10):103013, October 2011.

[7] B Geiger, M Garcia-Munoz, W W Heidbrink, R M McDermott, G Tardini, R Dux, R Fischer, and V Igochine. Fast-ion D-alpha measurements at ASDEX Upgrade. *Plasma Physics and Controlled Fusion*, 53(6):065010, June 2011.

[8] F Meo, H Bindslev, S B Korsholm, V Furtula, F Leuterer, F Leipold, P K Michelsen, S K Nielsen, M Salewski, J Stober, D Wagner, and P Woskov. Commissioning activities and first results from the collective Thomson scattering diagnostic on ASDEX Upgrade (invited). *The Review of scientific instruments*, 79(10):10E501, October 2008.

[9] M. Salewski, F. Meo, M. Stejner, O. Asunta, H. Bindslev, V. Furtula, S. B. Korsholm, T. Kurki-Suonio, F. Leipold, F. Leuterer, P. K. Michelsen, D. Moseev, S. K. Nielsen, J. Stober, G. Tardini, D. Wagner, and P. Woskov. Comparison of fast ion collective Thomson scattering measurements at ASDEX Upgrade with numerical simulations. *Nuclear Fusion*, 50(3):035012, March 2010.

[10] F. Meo, M. Stejner, M. Salewski, H. Bindslev, T. Eich, V. Furtula, S. B. Korsholm, F. Leuterer, F. Leipold, P. K. Michelsen, D. Moseev, S. K. Nielsen, B. Reiter, J. Stober, D. Wagner, P. Woskov, and The Asdex Upgrade Team. First results and analysis of collective Thomson scattering (CTS) fast ion distribution measurements on ASDEX Upgrade. *Journal of Physics: Conference Series*, 227:012010, May 2010.

[11] V Furtula, M Salewski, F Leipold, P K Michelsen, S B Korsholm, F Meo, D Moseev, S K Nielsen, M Stejner, and T Johansen. Design and performance of the collective Thomson scattering receiver at ASDEX Upgrade. *The Review of scientific instruments*, 83(1):013507, January 2012.

[12] V Furtula, F Leipold, M Salewski, P K Michelsen, S B Korsholm, F Meo, D Moseev, S K Nielsen, M Stejner, and T Johansen. Performance measurements of the collective Thomson scattering receiver at ASDEX Upgrade. *Journal of Instrumentation*, 7(02):C02039–C02039, February 2012.

[13] M. Salewski, B. Geiger, S.K. Nielsen, H. Bindslev, M. García-Muñoz, W.W. Heidbrink, S.B. Korsholm, F. Leipold, F. Meo, P.K. Michelsen, D. Moseev, M. Stejner, and G. Tardini. Tomography of fast-ion velocity-space distributions from synthetic CTS and FIDA measurements. *Nuclear Fusion*, 52(10):103008, October 2012.

[14] L Giacomelli, A Zimbal, K Tittelmeier, H Schuhmacher, G Tardini, and R Neu. The compact neutron spectrometer at ASDEX Upgrade. *The Review of scientific instruments*, 82(12):123504, December 2011.

[15] G Tardini, A Zimbal, B Esposito, F Gagnon-Moisan, D Marocco, R Neu, H Schuhmacher, and the ASDEX Upgrade Team. First neutron spectrometry measurements in the ASDEX Upgrade tokamak. *Journal of Instrumentation*, 7(03):C03004–C03004, March 2012.

[16] T. Kurki-Suonio, V. Hynönen, W. Suttrop, H.-U. Fahrbach, Stober. J., and the ASDEX Upgrade

Team. Edge Fast Ion Distribution benchmarking ASCOT against experimental NPA data on ASDEX Upgrade. In *Europhysics Conference Abstracts 30I*, page P2.145, 2006.

[17] S Äkäslompolo, E Hirvijoki, T Kurki-Suonio, and the ASDEX Upgrade Team. Implementing beam-beam CX-reactions in the ASCOT-code and prediction of active NPA measurement. In *Europhysics Conference Abstracts 34A*, page P5.113, 2010.

[18] M. Nocente, M. Garcia-Munoz, G. Gorini, M. Tardocchi, A. Weller, S. Akaslompolo, R. Bilato, V. Bobkov, C. Cazzaniga, B. Geiger, G. Grosso, A. Herrmann, V. Kiptily, M. Maraschek, R. McDermott, J.M. Noterdaeme, Y. Podoba, G. Tardini, and the ASDEX Upgrade Team. Gamma-ray spectroscopy measurements of confined fast ions on asdex upgrade. *Nuclear Fusion*, 52(9):094021, 2012.

[19] D. Moseev, F. Meo, S. B. Korsholm, T. Koskela, M. Albergante, O. Asunta, H. Bindslev, A. Bürger, V. Furtula, M. Yu. Kantor, F. Leipold, P. K. Michelsen, S. K. Nielsen, M. Salewski, O. Schmitz, M. Stejner, and E. Westerhof. Comparison of measured and simulated fast ion velocity distributions in the TEXTOR tokamak. *Plasma Physics and Controlled Fusion*, 53(10):105004, October 2011.

[20] W W Heidbrink. Fast-ion Dα measurements of the fast-ion distribution (invited). *The Review of scientific instruments*, 81(10):10D727, October 2010.

[21] A.C. Kak and M. Slaney. *Principles of Computerized Tomographic Imaging*. IEEE Press, 1988.

[22] G.T. Herman. *Fundamentals of Computerized Tomography*. Springer, 2nd edition, 2009.

[23] K Ertl, W. von der Linden, V Dose, and A Weller. Maximum entropy based reconstruction of soft X-ray emissivity profiles in W7-AS. *Nuclear Fusion*, 36(11):1477–1488, November 1996.

[24] M Anton, H Weisen, M J Dutch, W von der Linden, F Buhlmann, R Chavan, B Marletaz, P Marmillod, and P Paris. X-ray tomography on the TCV tokamak. *Plasma Physics and Controlled Fusion*, 38(11):1849–1878, November 1996.

[25] L.C Ingesson, B Alper, H Chen, A.W Edwards, G.C Fehmers, J.C Fuchs, R Giannella, R.D Gill, L Lauro-Taroni, and M Romanelli. Soft X ray tomography during ELMs and impurity injection in JET. *Nuclear Fusion*, 38(11):1675–1694, November 1998.

[26] Y Nagayama, G Taylor, M Yamada, E.D Fredrickson, A.C Janos, and K.M McGuire. ECE image reconstruction of partial sawtooth crashes in ohmic plasmas. *Nuclear Fusion*, 36(4):521–526, April 1996.

[27] John Howard. Vector tomography applications in plasma diagnostics. *Plasma Physics and Controlled Fusion*, 38(4):489–503, April 1996.

[28] S Konoshima, A W Leonard, T Ishijima, K Shimizu, I Kamata, W H Meyer, S Sakurai, H Kubo, N Hosogane, and H Tamai. Tomographic reconstruction of bolometry for JT-60U diverted tokamak characterization. *Plasma Physics and Controlled Fusion*, 43(7):959–983, July 2001.

[29] B J Peterson, A Yu Kostrioukov, N Ashikawa, Y Liu, Yuhong Xu, M Osakabe, K Y Watanabe, T Shimozuma, S Sudo, and the LHD Experiment Group. Bolometer diagnostics for one- and two-dimensional measurements of radiated power on the Large Helical Device. *Plasma Physics and Controlled Fusion*, 45(7):1167–1182, July 2003.

[30] I Furno, H Weisen, C Carey, C Angioni, R Behn, E Fable, A Zabolotsky, the TCV Team, and JET-EFDA Contributors. A new method for the inversion of interferometry data using basis functions derived from singular value decomposition of local measurements in tokamak plasmas. *Plasma Physics and Controlled Fusion*, 47(1):49–69, January 2005.

[31] G Bonheure, S Popovichev, L Bertalot, A Murari, S Conroy, J Mlynar, I Voitsekhovitch, and JET-EFDA Contributors. Neutron profiles and fuel ratio n T / n D measurements in JET ELMy H-mode plasmas with tritium puff. *Nuclear Fusion*, 46(7):725–740, July 2006.

[32] J Svensson and A Werner. Current tomography for axisymmetric plasmas. *Plasma Physics and Controlled Fusion*, 50(8):085002, August 2008.

[33] J. Egedal and H. Bindslev. Reconstruction of gyrotropic phase-space distributions from one-dimensional projections. *Physics of Plasmas*, 11(5):2191, April 2004.

[34] M. Salewski, S.K. Nielsen, H. Bindslev, V. Furtula, N. N. Gorelenkov, S. B. Korsholm, F. Leipold,

F. Meo, P. K. Michelsen, D. Moseev, and M. Stejner. On velocity space interrogation regions of fast-ion collective Thomson scattering at ITER. *Nuclear Fusion*, 51(8):083014, 2011.

[35] S. K. Nielsen, H. Bindslev, M. Salewski, A. Bürger, E. Delabie, V. Furtula, M. Kantor, S. B. Korsholm, F. Leipold, F. Meo, P. K. Michelsen, D. Moseev, J. W. Oosterbeek, M. Stejner, E. Westerhof, and P. Woskov. Fast-ion redistribution due to sawtooth crash in the TEXTOR tokamak measured by collective Thomson scattering. *Plasma Physics and Controlled Fusion*, 52(9):092001, September 2010.

[36] S. K. Nielsen, M. Salewski, H. Bindslev, A. Bürger, V. Furtula, M. Kantor, S. B. Korsholm, H. R. Koslowski, A. Krämer-Flecken, F. Leipold, F. Meo, P. K. Michelsen, D. Moseev, J. W. Oosterbeek, M. Stejner, and E. Westerhof. Dynamics of fast ions during sawtooth oscillations in the TEXTOR tokamak measured by collective Thomson scattering. *Nuclear Fusion*, 51(6):063014, June 2011.

[37] D.C. Pace, R.K. Fisher, M. García-Muñoz, W.W. Heidbrink, G.R. McKee, M. Murakami, C.M. Muscatello, R. Nazikian, J.M. Park, C.C. Petty, T.L. Rhodes, G.M. Staebler, M.A. Van Zeeland, R.E. Waltz, R.B. White, J.H. Yu, W. Zhang, and Y.B. Zhu. Transport of energetic ions due to sawteeth, Alfvén eigenmodes and microturbulence. *Nuclear Fusion*, 51(4):043012, April 2011.

[38] C M Muscatello, W W Heidbrink, Ya I Kolesnichenko, V V Lutsenko, M A Van Zeeland, and Yu V Yakovenko. Velocity-space studies of fast-ion transport at a sawtooth crash in neutral-beam heated plasmas. *Plasma Physics and Controlled Fusion*, 54(2):025006, February 2012.

[39] W.W Heidbrink and G.J Sadler. The behaviour of fast ions in tokamak experiments. *Nuclear Fusion*, 34(4):535–615, April 1994.

[40] S.J Zweben, R.V Budny, D.S Darrow, S.S Medley, R Nazikian, B.C Stratton, E.J Synakowski, and G. Taylor for the TFTR Group. Alpha particle physics experiments in the Tokamak Fusion Test Reactor. *Nuclear Fusion*, 40(1):91–149, January 2000.

[41] F. Nabais, D. Borba, M. Garcia-Muñoz, T. Johnson, V.G. Kiptily, M. Reich, M.F.F. Nave, S.D. Pinches, and S.E. Sharapov. Impact of strongly driven fishbones and Alfvén Eigenmodes on fast ion losses. *Nuclear Fusion*, 50(11):115006, November 2010.

[42] M. A. Van Zeeland, W. W. Heidbrink, R. K. Fisher, M. Garcia Munoz, G. J. Kramer, D. C. Pace, R. B. White, S. Aekaeslompolo, M. E. Austin, J. E. Boom, I. G. J. Classen, S. da Graca, B. Geiger, M. Gorelenkova, N. N. Gorelenkov, A. W. Hyatt, N. Luhmann, M. Maraschek, G. R. McKee, R. A. Moyer, C. M. Muscatello, R. Nazikian, H. Park, S. Sharapov, W. Suttrop, G. Tardini, B. J. Tobias, and Y. B. Zhu. Measurements and modeling of Alfven eigenmode induced fast ion transport and loss in DIII-D and ASDEX Upgrade. *Physics of Plasmas*, 18(5):056114, May 2011.

[43] D C Pace, R K Fisher, M García-Muñoz, W W Heidbrink, and M A Van Zeeland. Convective beam ion losses due to Alfvén eigenmodes in DIII-D reversed-shear plasmas. *Plasma Physics and Controlled Fusion*, 53(6):062001, June 2011.

[44] S Günter, G Conway, S DaGraça, H.-U Fahrbach, C Forest, M. Garcia Muñoz, T Hauff, J Hobirk, V Igochine, F Jenko, K Lackner, P Lauber, P McCarthy, M Maraschek, P Martin, E Poli, K Sassenberg, E Strumberger, G Tardini, E Wolfrum, H Zohm, and ASDEX Upgrade Team. Interaction of energetic particles with large and small scale instabilities. *Nuclear Fusion*, 47(8):920–928, August 2007.

[45] T. Dannert, S. Gunter, T. Hauff, F. Jenko, X. Lapillonne, and P. Lauber. Turbulent transport of beam ions. *Physics of Plasmas*, 15(6):062508, June 2008.

[46] T. Hauff and F. Jenko. Mechanisms and scalings of energetic ion transport via tokamak microturbulence. *Physics of Plasmas*, 15(11):112307, November 2008.

[47] T. Hauff, M. Pueschel, T. Dannert, and F. Jenko. Electrostatic and magnetic transport of energetic ions in turbulent plasmas. *Physical Review Letters*, 102(7), February 2009.

[48] J P Graves, I T Chapman, S Coda, M Lennholm, M Albergante, and M Jucker. Control of magnetohydrodynamic stability by phase space engineering of energetic ions in tokamak plasmas. *Nature communications*, 3:624, January 2012.

[49] S Kubo, M Nishiura, K Tanaka, T Shimozuma, Y Yoshimura, H Igami, H Takahash, T Mutoh, N Tamura, Y Tatematsu, T Saito, T Notake, S B Korsholm, F Meo, S K Nielsen, M Salewski, and M Stejner. Collective Thomson scattering of a high power electron cyclotron resonance heating beam in LHD (invited). *The Review of scientific instruments*, 81(10):10D535, October 2010.

[50] Takafumi ITO, Masaki OSAKABE, Katsumi IDA, Mikiro YOSHINUMA, Masahiko KOBAYASHI, Sadayoshi MURAKAMI, Motoshi GOTO, Yasuhiko TAKEIRI, Detlev REITER, and Shoichi OKAMURA. Effect of Halo Neutrals on Fast-Ion Charge Exchange Spectroscopy Measurements in LHD. *Plasma and Fusion Research*, 5:S2099, 2012.

[51] A. Kappatou, E. Delabie, R.J.E. Jaspers, and M.G. von Hellermann. Feasibility of non-thermal helium measurements with charge exchange spectroscopy on ITER. *Nuclear Fusion*, 52(4):043007, April 2012.

[52] M Salewski, F Meo, H Bindslev, V Furtula, S B Korsholm, B Lauritzen, F Leipold, P K Michelsen, S K Nielsen, and E Nonbø l. Investigation of first mirror heating for the collective Thomson scattering diagnostic in ITER. *The Review of scientific instruments*, 79(10):10E729, October 2008.

[53] M. Salewski, O. Asunta, L.-G. Eriksson, H. Bindslev, V. Hynönen, S. B. Korsholm, T. Kurki-Suonio, F. Leipold, F. Meo, P. K. Michelsen, S. K. Nielsen, and J. Roenby. Comparison of collective Thomson scattering signals due to fast ions in ITER scenarios with fusion and auxiliary heating. *Plasma Physics and Controlled Fusion*, 51(3):035006, March 2009.

[54] M. Salewski, L.-G. Eriksson, H. Bindslev, S.B. Korsholm, F. Leipold, F. Meo, P.K. Michelsen, and S.K. Nielsen. Impact of ICRH on the measurement of fusion alphas by collective Thomson scattering in ITER. *Nuclear Fusion*, 49(2):025006, February 2009.

[55] F Leipold, V Furtula, M Salewski, H Bindslev, S B Korsholm, F Meo, P K Michelsen, D Moseev, S K Nielsen, and M Stejner. Antenna design for fast ion collective Thomson scattering diagnostic for the international thermonuclear experimental reactor. *The Review of scientific instruments*, 80(9):093501, September 2009.

[56] W W Heidbrink, Y Luo, K H Burrell, R W Harvey, R I Pinsker, and E Ruskov. Measurements of fast-ion acceleration at cyclotron harmonics using Balmer-alpha spectroscopy. *Plasma Physics and Controlled Fusion*, 49(9):1457–1475, September 2007.

[57] W.W. Heidbrink, M.A. Van Zeeland, M.E. Austin, K.H. Burrell, N.N. Gorelenkov, G.J. Kramer, Y. Luo, M.A. Makowski, G.R. McKee, C. Muscatello, R. Nazikian, E. Ruskov, W.M. Solomon, R.B. White, and Y. Zhu. Central flattening of the fast-ion profile in reversed-shear DIII-D discharges. *Nuclear Fusion*, 48(8):084001, August 2008.

[58] C M Muscatello, W W Heidbrink, D Taussig, and K H Burrell. Extended fast-ion D-alpha diagnostic on DIII-D. *The Review of scientific instruments*, 81(10):10D316, October 2010.

[59] A Bortolon, W W Heidbrink, and M Podestà. A tangentially viewing fast ion D-alpha diagnostic for NSTX. *The Review of scientific instruments*, 81(10):10D728, October 2010.

[60] R. J. Barlow. *Statistics*. Wiley, 1989.

[61] E. H. Moore. THE FOURTEENTH WESTERN MEETING OF THE AMERICAN MATHEMATICAL SOCIETY. *Bulletin of the American Mathematical Society*, 26:385–396, 1920.

[62] R. Penrose. A generalized inverse for matrices. *Mathematical Proceedings of the Cambridge Philosophical Society*, 51(03):406–413, July 1955.

[63] G. Strang. *Linear Algebra and its Applications*. Harcourth Brace Jovanovich, 1988.

[64] M. Stejner, S. K. Nielsen, S. B. Korsholm, M. Salewski, H. Bindslev, V. Furtula, F. Leipold, F. Meo, P. K. Michelsen, D. Moseev, A. Burger, M. Kantor, and M. de Baar. Collective Thomson scattering measurements with high frequency resolution at TEXTOR. *Review of Scientific Instruments*, 81(10):10D515, 2010.

[65] S. B. Korsholm, M. Stejner, H. Bindslev, V. Furtula, F. Leipold, F. Meo, P. Michelsen, D. Moseev, S. Nielsen, M. Salewski, M. de Baar, E. Delabie, M. Kantor, and A. Bürger. Measurements of

Intrinsic Ion Bernstein Waves in a Tokamak by Collective Thomson Scattering. *Physical Review Letters*, 106(16):165004, April 2011.

[66] M Stejner, S B Korsholm, S K Nielsen, M Salewski, H Bindslev, S Brezinsek, V Furtula, F Leipold, P K Michelsen, F Meo, D Moseev, A Bürger, M Kantor, and M de Baar. Measurements of plasma composition in the TEXTOR tokamak by collective Thomson scattering. *Plasma Physics and Controlled Fusion*, 54(1):015008, January 2012.